A climatology of infrasound detections in northern Norway at the experimental ARCI array

Läslo Gerardus Evers, Johannes Schweitzer

J Seismol
DOI 10.1007/s10950-011-9237-8

ORIGINAL ARTICLE

A climatology of infrasound detections in northern Norway at the experimental ARCI array

Läslo Gerardus Evers · Johannes Schweitzer

Received: 20 August 2009 / Accepted: 17 March 2011

Abstract The study of infrasound is experiencing a renaissance in recent years since it was chosen as a verification technique for the Comprehensive Nuclear-Test-Ban Treaty. Currently, 60 infrasound arrays are being installed to monitor the atmosphere for nuclear tests as part of the International Monitoring System (IMS). The number of non-IMS arrays also increases worldwide. The experimental ARCES infrasound array (ARCI) is an example of such an initiative. The detectability of infrasound differs for each array and is a function of the array location and configuration, the state of the atmosphere, and the presence of natural and anthropogenic sources. In this study, a year of infrasound data is analyzed as recorded by ARCI. Contributions of the atmosphere and the sources are evaluated in both a low- (0.1–1.0 Hz) and high-frequency (1.0–7.0 Hz) passband. The enormous number of detections in the low-frequency band is explained in terms of the stratospheric wind and ocean wave activity and compared with the detection of microseism. Understanding the detectability in the low-frequency band is of utmost importance for successfully applying infrasound as a verification technique since small-sized nuclear test will show up in this frequency range.

Keywords Infrasound · Array · Signal detection · Source identification · Acoustic propagation

1 Introduction

Infrasound was first discovered after the violent eruption of the Krakatoa, Indonesia, in 1883. Low-frequency pressure waves were observed at traditional barographs. These appeared to have traveled with the sound speed and up to four passages where noticed at some instruments (Symons 1888). The first microbarometer recordings date from 1908 when a comet, or asteroid, exploded over Siberia in Russia, the so-called Tunguska event (Whipple 1930). The societal and scientific interest in infrasound increased during World War I, e.g., Whipple (1939), and later on in the nuclear testing era (Posey and Pierce 1971). With the

L. G. Evers
Seismology Division, Royal Netherlands Meteorological Institute, PO Box 201, 3730 AE De Bilt, The Netherlands

L. G. Evers (✉)
Acoustic Remote Sensing Group, Faculty of Aerospace Engineering, TU Delft, PO Box 5, 2600 AA Delft, The Netherlands
e-mail: evers@knmi.nl

J. Schweitzer
NORSAR, PO Box 53, 2027 Kjeller, Norway
e-mail: johannes@norsar.no

signature of the Limited Test Ban Treaty in 1963, most interest in infrasound promptly came to a stop, since nuclear tests were confined to the subsurface. Only a few studies could be maintained (Balachandran et al. 1977; Liszka 1978). In recent years, the study of infrasound gained renewed interest because of the Comprehensive Nuclear-Test-Ban Treaty (CTBT) that opened for signing in 1996, where it is used as a verification technique for atmospheric tests (Dahlman et al. 2009).

Sources of infrasound are in general large, since an enormous amount of air has to be displaced to generate such low frequencies (Gossard and Hooke 1975). Natural sources are avalanches, lightning, meteors, oceanic waves, earthquakes, severe weather, volcanoes, and sprites. Among anthropogenic sources are explosions, supersonic flights, military activity, rocket launches, and nuclear tests. Identifying the sources of infrasound out of this zoo of coherent waves in the atmosphere is one of the major challenges in infrasound research.

The propagation of infrasound through the highly dynamic atmosphere plays an important role in source identification. Infrasound travels up to thermospheric altitudes of 120 km and experiences refractions due to an increase in wind and/or temperature as a function of altitude. If the gradients in the propagation velocity are strong enough, infrasound will be sent back to the Earth's surface (Drob et al. 2003). There are three regions in the atmosphere where such gradients might exist. These are of importance in long-range sound propagation, i.e., over distances larger than 150 km. The regions are marked by (1) a strong jet stream at 10 km altitude, near the tropopause; (2) the combined effect of wind and temperature at the stratopause, around 50 km altitude; and (3) the temperature increase in the thermosphere from 100 km and upward.

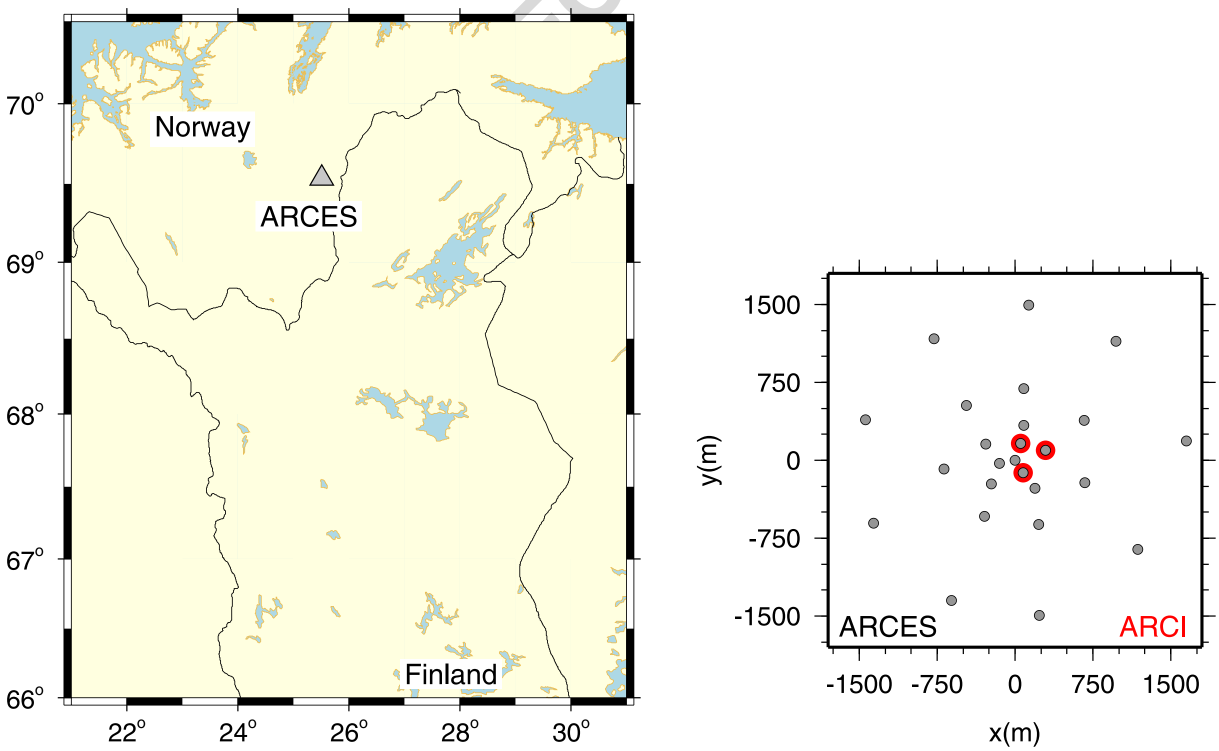

Fig. 1 The location of the ARCES seismic array and positions of the seismometers (*gray dots*). The temporary array ARCI is configured with three microbarometers (*red circles*), which are co-located with seismometers in the center of the seismic array

The aim of this study is to identify the sources around the ARCES array and to build up a climatology of station-specific detections. Each infrasound array has its own detection capabilities as its configuration, the atmospheric conditions, and source characteristics are highly variable as function of geographical location and time. Special attention will be paid to the low-frequency band of 0.1 to 1.0 Hz which is of utmost importance for the verification of the CTBT as small-sized nuclear tests (around 1 kT TNT) are expected to generate infrasound of 0.1 to 0.2 Hz (Evers and Haak 2001). It is also this band in which the almost continuous background noise of microbaroms is present that peak around 0.2 Hz (Posmentier 1967).

2 The ARCES infrasound array

A three-element experimental infrasound array was established at ARCES in March 2008, which will be abbreviated as ARCI (Roth et al. 2008). The purpose of the installation is to gain experience with the simultaneous recording of infrasonic and seismological data. Figure 1 shows the location and configuration of ARCI. The instruments are microbarometers of type Martec MB2005 which have a flat frequency response to pressure in the range of 0.01 to 27 Hz. Infrasound measurements are affected by noise due to wind. Therefore, a spatial filter is applied at each instrument which essentially integrates the pressure field. Doing so, pressure fluctuations with a small coherency length, like those of tens of centimeters associated with wind noise, are partly canceled out. The infrasonic waves of interest remain undisturbed because of their much larger coherency length of tens to hundreds of meters. Such analog filters can consist of a pipe array with discrete inlets or porous hoses (Hedlin et al 2003). The latter approach is applied at ARCI with four soaker hoses, each with a length of 12 m, connected to the MB2005. For one of the three sites, the hoses are additionally centered in a drainage pipe. Environmental restrictions at the ARCES array prevent the installation of larger pipe arrays that require fencing. The applied noise reduction should be considered as minimal. The atmospheric pressure changes around ARCI are sampled at a rate of 80 Hz.

3 Data processing and signal detection

3.1 The approach

The detections of coherent infrasonic signals traveling over the array can be achieved by evaluating the Fisher (F) ratio. The F detector has been described in both the time (Melton and Bailey 1957) and frequency domain (Smart and Flinn 1971). In essence, a statistical hypothesis is tested. Applying a F-detector is attractive because of its well-known statistical distribution. The hypothesis to be tested is that all recordings made by the microbarometers consist of uncorrelated noise. The alternative hypothesis is valid for the case that not only noise is present but also signal. Evaluated are the variance of the noise and the variance of all recordings, which cannot be attributed to the noise since it is common to all recordings. The F detector has been successfully applied in infrasound processing to detected, for example, meteors and microbaroms (Evers and Haak 2001). The processing sequence applied in this study is as follows:

– Remove the mean of the recordings.
– Band-pass filter with a second-order Butterworth filter with corner frequencies of 0.1 and 1.0 Hz (the low-frequency or microbarom band) and 1.0 and 7.0 (the high-frequency band).
– Decimate the data with a factor of 4, to reduce the data volume in order to minimize the computational efforts, from a 80- to 20-Hz sampling rate.
– Define a slowness grid between -0.005 and 0.005 s/m of 100 × 100 points, forming 10,000 beams.
– Split the data in segments of 256 samples, which equals a bin of 12.8 s.
– Evaluate the Fisher ratio for each beam in each bin (with 50% overlapping bins).
– Extract the slowness value, i.e., the backazimuth and apparent sound speed, at the maximum Fisher ratio, for each bin.

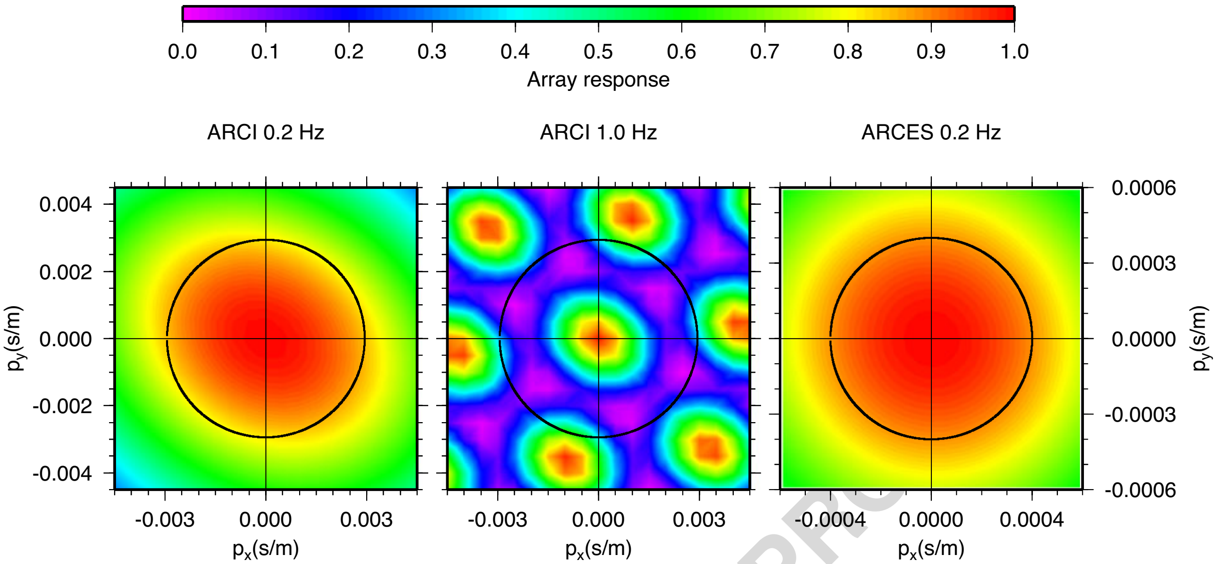

Fig. 2 The array response of ARCI to a 0.2- and 1.0-Hz planar wave (*left two frames*). The *black circle* represent an apparent velocity of 340 m/s. The array response of ARCES is given in the *right frame* at 0.2 Hz; the *black circle* corresponds to an apparent velocity of 2,500 m/s

The above approach extracts the most coherent arrival from a data segment. If multiple sources are active at the same time, preference is given to the one with the highest F ratio.

The array response of ARCI is given in Fig. 2 for a low (0.2 Hz) and higher frequent (1.0 Hz) planar wave. The limited aperture of ARCI results in a broad main lob at 0.2 Hz, but its maximum can still be confidently determined. At higher frequencies, spatial aliasing starts to play a role because of the low number of array elements. However, at 1.0 Hz, no side lobes are present in the velocity range of interest.

3.2 Detections in the high-frequency band

Most sources in the high-frequency band are man-made. Figure 3 shows the time of occurrence of events in this band, for the period of March 13, 2008 up to May 14, 2009. There appear to be less events during the weekends (days 6 and 7), compared to weekdays, and during nighttime. In other words, most events occur during the working week and at daytime hours, which clearly indicates that the sources are of anthropogenic origin. The resolved backazimuths with respect to ARCI are given in the left frame of Fig. 4. Most events occur from an eastern to southwestern direction. Some of these can be explained by quarries, mines, and military activity, as indicated by the red lines. The source of the peak around 190° has not yet been identified. Less events find their origin in the north, although two distinct peaks, around 290° and 330°, indicate activity to the northwest.

3.3 Detections in the low-frequency band

Figure 5 shows the results of the previously described processing approach for ARCI data in the low-frequency band between 0.1 and 1.0 Hz. The lower frame shows the maximum Fisher ratio for each bin. This value is related to the squared signal-to-noise ratio (SNR) on the traces (see axis on the right). The middle and top frames show the resolved apparent sound speed and backazimuth. Color coded are the number of detections within an hour, where five or more detections are denoted by red. Here, only detections with a SNR larger than 1.0 are plotted, which equals a Fisher ratio of four and higher. Such a detection

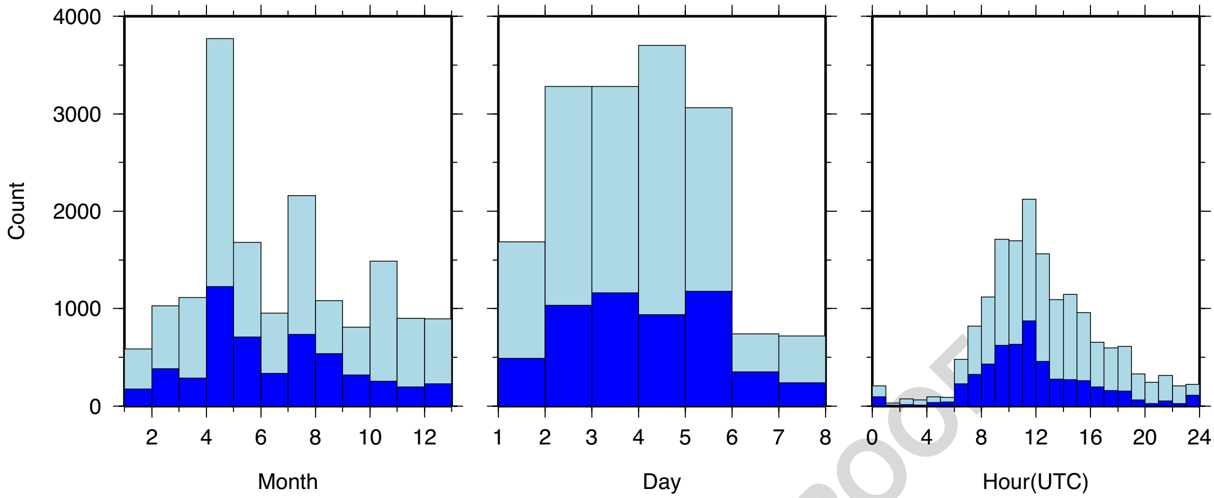

Fig. 3 Results from the array processing of ARCI data in the high-frequency band of 1.0 to 7.0 Hz. The histograms shows the time of occurrence of infrasound events, between March 13, 2008 and May 14, 2009. *Light blue colors* indicate events with an signal-to-noise ratio (SNR) larger than 1 (or Fisher ratio of 4 and higher). *Dark blue* means a SNR larger than 1.5. The weekday diagram starts with day 1 which is Monday. For the hour histogram, local time in Norway is UTC+2h for summer and UTC+1h for winter

will be labeled as an event and is mostly related to microbarom activity. It follows from the lower frame of Fig. 5 that signal coherency strongly fluctuates as function of time. Large changes are seen from day to day, but there also seems to be a difference between winter and summertime (May to September). These are also reflected in the resolved apparent sound speed and backazimuth. The short time variations in signal coherency show up as gaps, which means that no events have been detected. During summer, less coherent events are detected than in winter, and they appear from

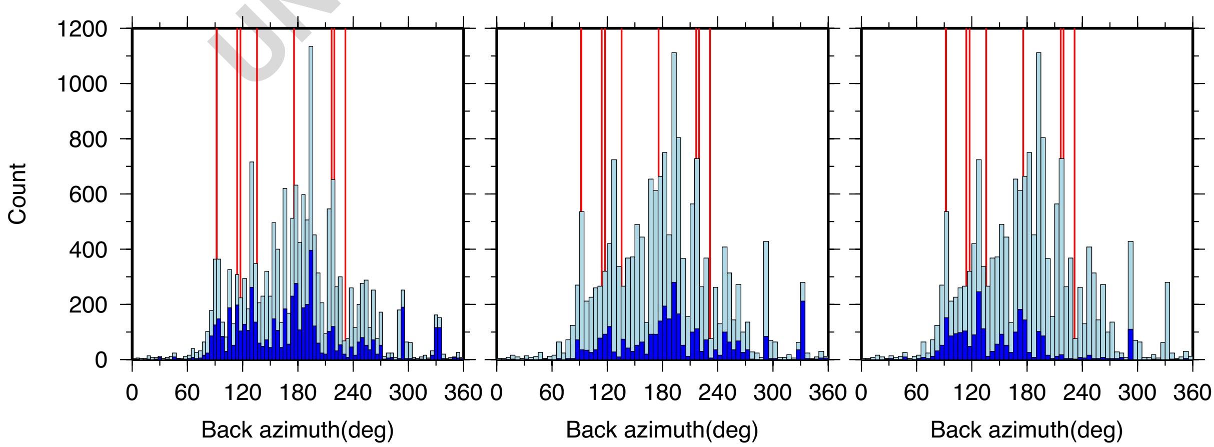

Fig. 4 The number of events (count) as function of the backazimuth for the high-frequency band. Events with a SNR larger than 1 are denoted by *light blue*; *blue* is used for a SNR larger than 1.5. The *red lines* give the backazimuths toward quarries, mines, and regions of military activity. The *left frame* gives all events; the *middle* and *right* frame are for winter and summer, respectively

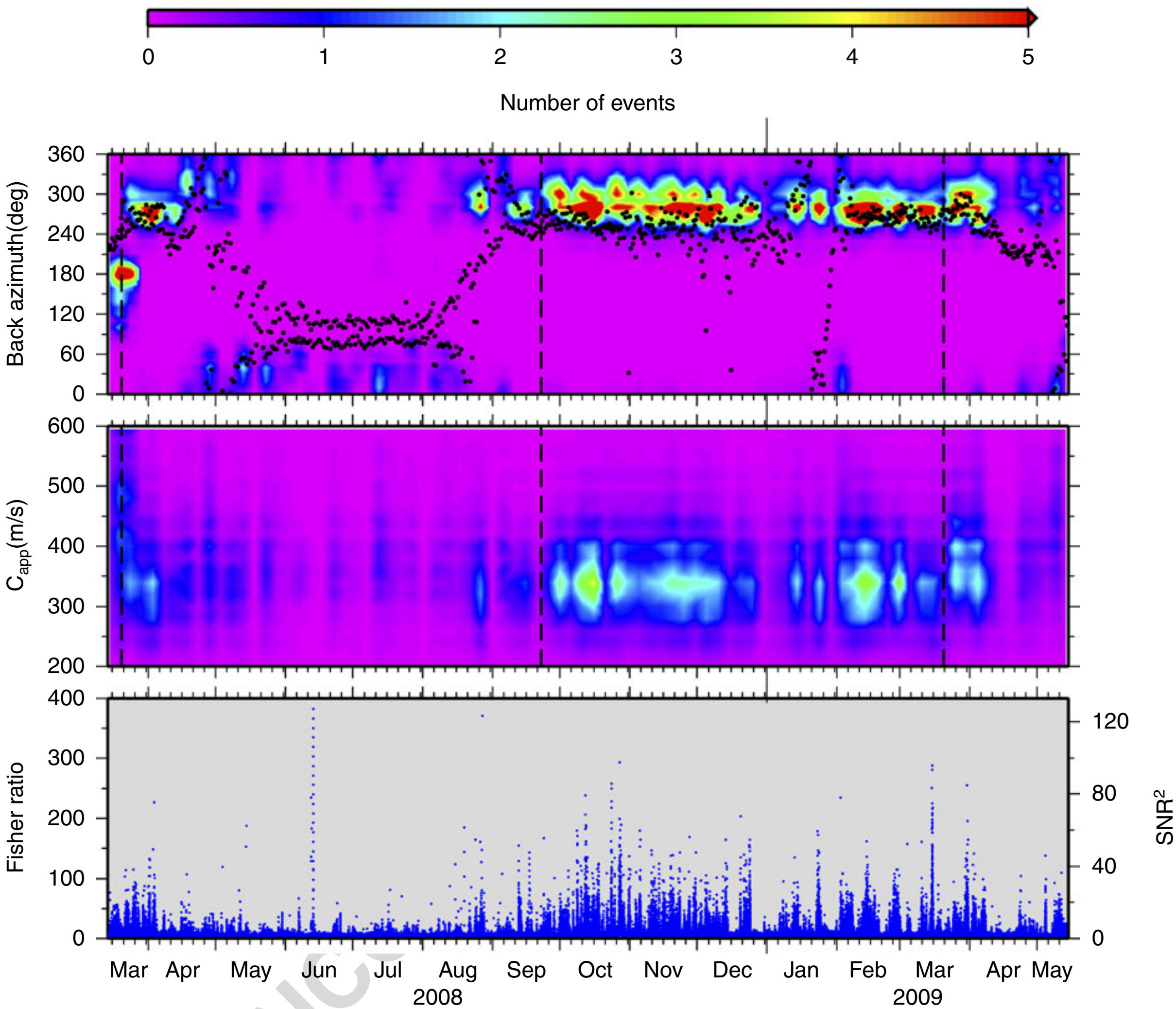

Fig. 5 Results from the array processing of ARCI data in the low-frequency band from 0.1 to 1.0 Hz. The *lower frame* shows the Fisher ratios as function of time, that is, between March 13, 2008 and May 14, 2009. The Fisher ratio is related to the signal-to-noise (SNR) power ratio on the traces (see the axis on the *right*). The *top frames* gives the resolved apparent sound speed and backazimuth. Color coded are the number events per hour with a SNR larger than 1. Five or more events are indicated by *red colors*. The *black dots* represent the wind direction at 50 km altitude from the ECMWF analysis at 69.50 N, 25.50 E. The equinoxes are indicated by the *vertical dashed lines* Q1

northeastern directions. In winter, events are detected almost continuously and find their origin to the west of ARCI.

Variations in the detectability of infrasound can have several causes. These could be related to the state of the atmosphere and variations of the source (Le Pichon et al. 2009; Evers and Haak 2005). For the atmosphere, contributions along the source–receiver path will be evaluated in the following as well as near receiver effects. The location, time, and strength of the source vary as function of time and will also be analyzed.

4 Contributions of the atmosphere

4.1 General propagation characteristics

Atmospheric causes of the variations in the detectability of infrasound are related to two distinct areas in the atmosphere, the stratosphere and the boundary layer. The boundary layer is approximately the first kilometer of atmosphere, within the lower troposphere. The stratosphere reaches from the tropopause, around 10 km, up to the stratopause near 50 km altitude. The thermosphere, from 100 km and upwards, is not considered here because, in the considered frequency range, thermospheric arrivals are strongly attenuated by the highly rarefied upper atmosphere. These are, therefore, not expected to be observed over ranges of over 1,000 km (Sutherland and Bass 2004).

4.2 Stratospheric variability

The wind in the stratosphere, called the polar vortex, varies on a seasonal scale. During winter, winds are directed to the east, around the stratopause on the Northern Hemisphere. These winds can reach values of over 150 m/s. In summer, these winds are directed to the west and somewhat less strong, reaching values of 70 m/s. Figure 6 shows the wind and temperature near ARCI, at 69.50 N, 25.50 E, as function of time. These atmospheric specifications were obtained from the European Centre for Medium-Range Weather Forecasts (ECMWF). The wind is split in a meridional and zonal component. The meridional wind is the south–north component of the wind and has a positive sign when directed to the north. A positive sign for the zonal wind, which is the west–east component, means it is directed to the east. The change in the zonal wind direction around the equinox should be noted, which causes the anisotropy of the medium.

The temperature increase, due to presence of ozone, and strong winds around 50 km altitude may lead to bending of infrasonic waves back to the Earth's surface, due to the increase in effective propagation velocity. Changes in this so-called stratospheric duct are visible in the surface based microbarometer recordings of ARCI.

4.2.1 Consequences for the high-frequency band

For the high-frequency band, a distinction is made between summer and winter in Fig. 4. It follows from this figure that events from the west are more easily detected in winter as the stratospheric winds are favorable for such propagation. Events from the east are better detected in summer, but some show up in wintertime. The detections of sources which are not affected by the direction of the polar vortex probably find their origin close to the array, i.e., at distances less than 150 km, where tropospheric propagation is still dominant.

4.2.2 Consequences for the low-frequency band

In Fig. 5, the wind direction at 50 km altitude is superimposed on the resolved backazimuths, for the low frequency band. Clearly, the detection of coherent infrasound is guided by the stratospheric wind. In winter, microbarom energy from the Northern Atlantic Ocean is recorded. As the winds turn around the equinox, microbarom energy from the east is being detected.

As can been seen in Fig. 6, an abrupt change in the winds and temperature occurred in the winter of 2009, between late January and early February. Such changes are related to a major sudden stratospheric warming (SSW; Holton 1979). The temperature increases by 50°C in the stratosphere, in only a couple of days, and the polar vortex changes its direction. The major SSW also had its effect on the infrasound detections (see also Fig. 5). Suddenly, microbaroms from the east are detected because of the change in direction of the polar vortex, which is unusual in winter (Evers and Siegmund 2009).

4.3 Variability in the boundary layer

The state of the boundary layer above the array can cause de-correlation of the signals. A turbulent atmosphere affects the signal coherency which leads to a decrease of the detection capability. The summer boundary layer is far more turbulent than the winter one. Heating of the boundary layer due to solar radiation generates a high degree of mixing. This effect is also visible on a daily scale where the nighttime boundary layer stabilizes as the influence of solar radiation decreases.

Figure 7 shows the signal coherency, by means of the Fisher ratio, for July and October 2008

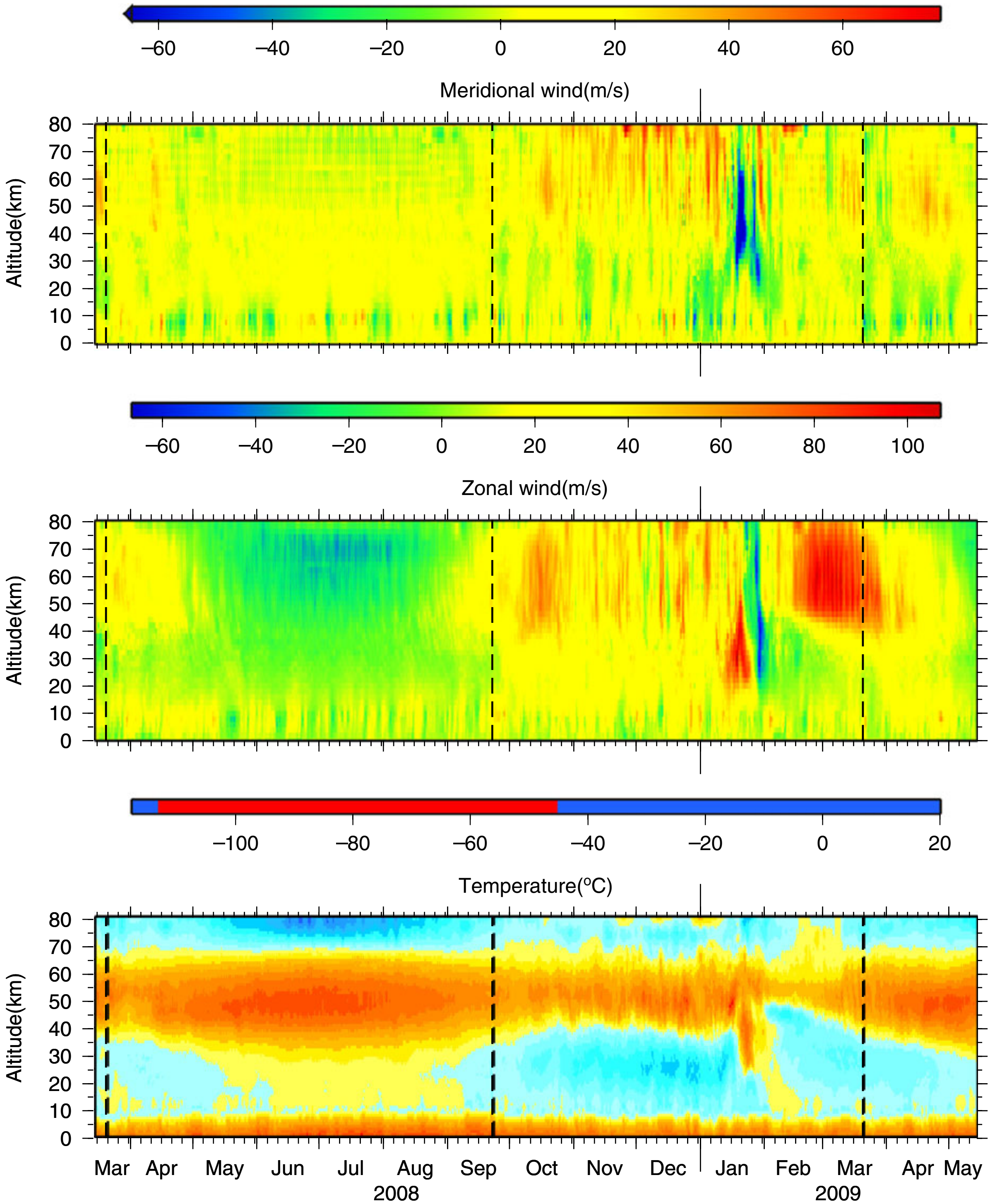

Fig. 6 The temperature and wind from the analyzes provided by the ECMWF. These models are available on a 0.5 × 0.5° grid, each 6 h/day. The grid node closest to ARCI is chosen, being 69.50 N, 25.50 E. The wind and temperature is modeled at 91 levels up to an altitude of approximately 80 km. All values for the meridional wind lower than −65 m/s are colored *blue*, for plotting purposes, the actual lowest value is −140 m/s. The equinoxes are indicated by the *vertical dashed lines* Q1

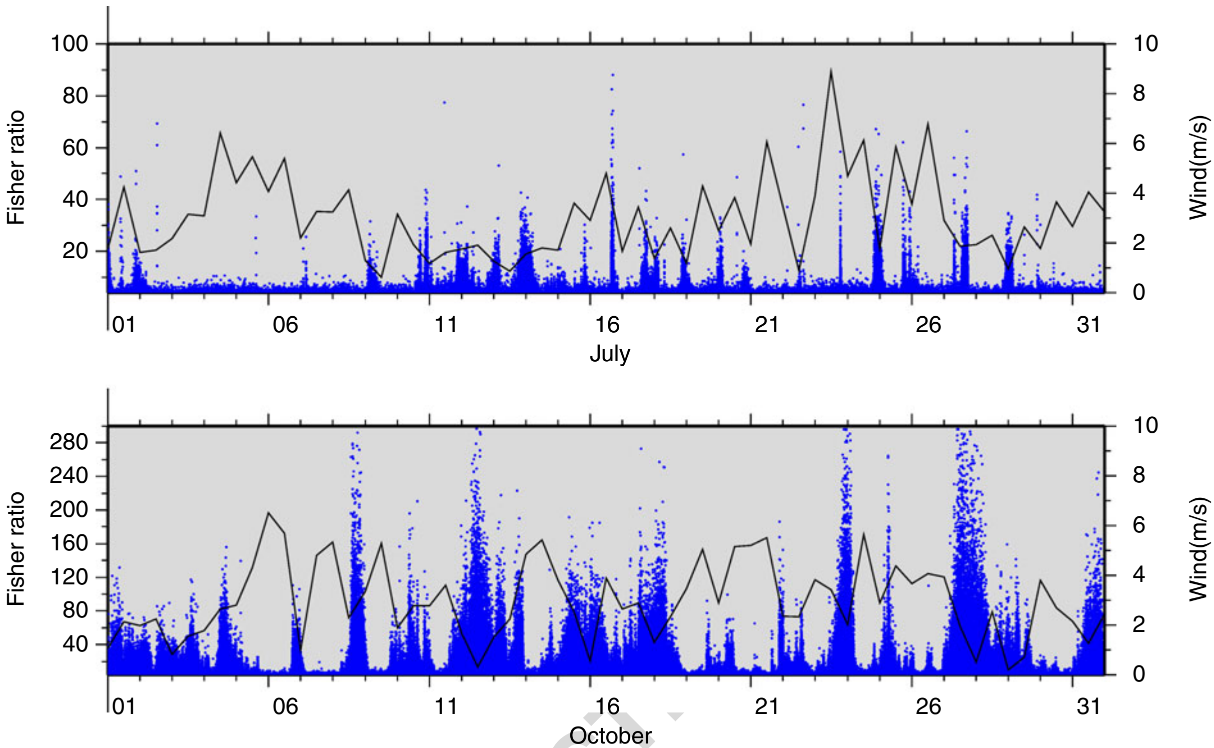

Fig. 7 The Fisher ratios for July (*top*) and October 2008 (*bottom frame*), for the low-frequency band. Superimposed are the wind strengths, as *solid black lines*, at the first level of the ECMWF models at 69.50 N, 25.5 E. This first level corresponds to an altitude slightly above the Earth's surface Q1

in the low-frequency band. Superimposed are the wind strengths from ECMWF models, at 69.50 N, 25.50 E, for the first level which is slightly, i.e., around 300 m, above the Earth's surface. It follows from this figure that the wind strength in summer varies on a daily basis. It peaks during daytime and decreases at night when the influence of solar radiation is reduced. The reduction in wind leads to an increase in the detectability of infrasound which is reflected by higher Fisher ratios. Wind variations in winter have longer periods, but also here an increase in wind leads to a decrease in performance of the array.

5 Specifications of the microbarom sources

5.1 Description of microbarom source

The source generating the signals, in the low-frequency band, varies in strength over time. The microbaroms are generated by the non-linear interaction of oceanic waves, which often occurs in the vicinity of low-pressure systems over the oceans. The interference of almost oppositely traveling waves leads to pressure signals in both the atmosphere and the solid Earth, i.e., microseism. The signals have a dominant frequency around 0.2 Hz, which is double the frequency of the oceanic waves. The amplitude of induced pressure waves (I_S) is, in first order, proportional to the squared multiplication of the wave height (a) and frequency (ω), thus $I_S \sim (a\omega)^2$ (Posmentier 1967). To accurately predict the generation of microbaroms, the directional spectra of oceanic waves should be evaluated to identify the almost oppositely traveling waves and their periods (Kedar et al. 2008). Here, it is assumed that the waves are interacting near the maximum of the squared multiplication of the wave height and frequency. This allows for an efficient calculation, to get an indication of the source activity (Evers and Haak 2001). An independent approach will also be tested where the occurrence of microseism in the seismic recordings of ARCES are evaluated.

5.2 Wave height and frequency from oceanic wave models

Figure 8 shows the backazimuths in the direction of microbarom activity in the Atlantic and Pacific Ocean, from 12-hourly oceanic wave models provided by the ECMWF. The source intensity, I_S, is also estimated. The observed backazimuths of the infrasound and direction of microbarom activity coincide throughout the seasons. The detection of microbaroms is also clearly related to the direction of the stratospheric winds (Garcés et al. 2004; Le Pichon et al. 2006). During the SSW which occurred in the winter of 2009, there is a sudden change in resolved backazimuths. Microbarom energy from the Pacific Ocean is detected, during

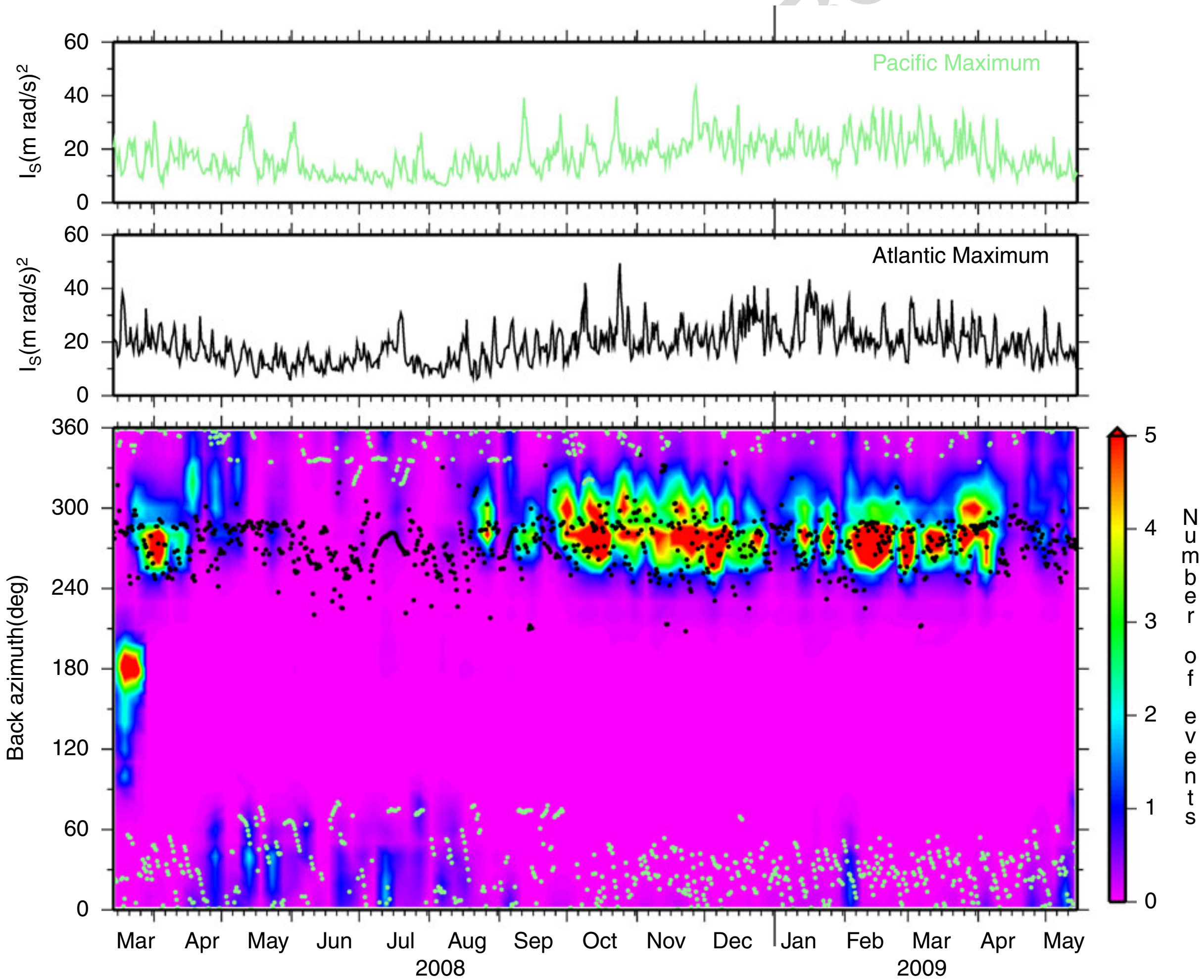

Fig. 8 An estimate of the microbarom activity in the Atlantic (*black dots*) and Pacific Ocean (*green dots*). The *dots* give the directions, i.e., backazimuths, to the Atlantic and Pacific maxima. The retrieved directions, in the *lower frame*, and source intensities (I_S, in the *upper frames*) are calculated from 12-hourly oceanic wave models from ECMWF provided at each 0.5 × 0.5°

Q1

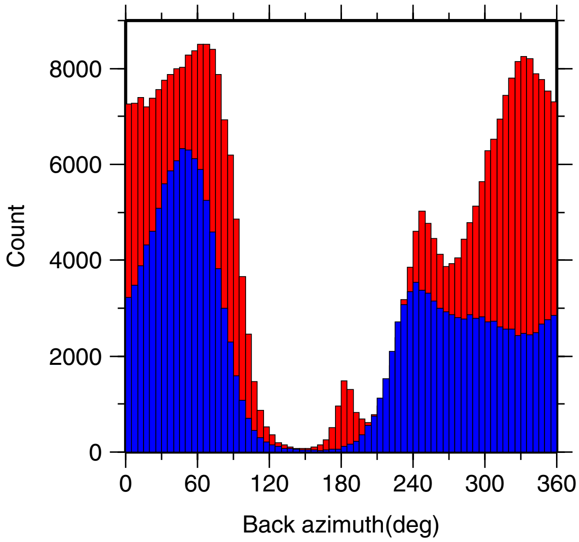

Fig. 9 Detections of microseism at the ARCES array. These detections are split in summer (in *red*, April through September) and winter (*blue*)

a short period in early February. This indicates that the low-frequency energy detected during summer might also find its origin on the Pacific Ocean.

5.3 Comparison with microseismic detections

Seismic data from the ARCES array (see Fig. 1) are processed to detect energy from microseism. The processing sequence is as follows:

- Band-pass filter with a third-order Butterworth filter with corner frequencies of 0.1 and 0.4 Hz.
- Decimate the data with a factor of 8, from a 40- to 5-Hz sampling rate.
- Split the data in a window of 20 s.
- Apply a frequency–wavenumber analysis, between 0.15 and 0.25 Hz, by moving this window with 6 s.
- Calculate a beam and measure the maximum amplitude in the window.

The array response of ARCES for a 0.2-Hz planar wave is given in Fig. 2. At such low frequencies, the main lob is quite broad but its maximum can still be determined with enough accuracy for this study, since only a rough estimate ($\pm 5°$) of the backazimuth is sufficient. The detections of microseism at ARCES are shown in Fig. 9. A total of 6.4 million coherent seismic arrivals are detected between 0.15 and 0.25 Hz. This number is

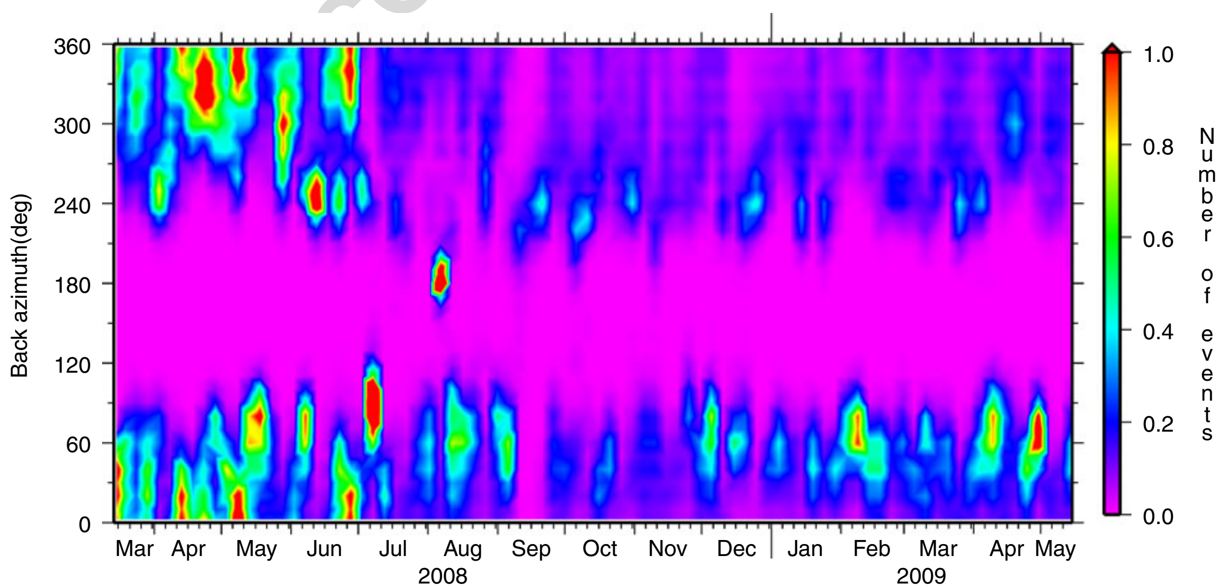

Fig. 10 The occurrence of microseism at the ARCES array. Detections are contoured as function of time and backazimuth. The detections are averaged per hour and one or more detections are indicated by *red colors*

significantly reduced by only considering apparent velocities between 2.0 and 3.0 km/s, which resembles the Rayleigh wave propagation velocity. A further reduction is achieved by only allowing for detections with a large signal coherency. The signal coherency is determined by the normalized frequency–wavenumber spectrum. If a threshold of 0.8 is chosen for the spectral density, the number of detections is reduced to 494,290. No energy appears at ARCES from roughly a south to southeastern direction, as expected from its geographical location. Microseism are present from the east to the west, via the north, indicating local and distant ocean wave activity, i.e., the North Atlantic and north of the Siberian coastline when the Arctic is not covered by sea ice or eventually from the northern Pacific Ocean. A peak pops up around 180° during summer (April through September).

The microseismic detections are represented as function of time in Fig. 10, in a similar way as the microbaroms (see Fig. 5). Microseismic energy is almost continuously being detected probably from nearby sources and the Atlantic, the Arctic, and possibly the Pacific Oceans. Microbarom detections, on the other hand, showed a strong directionality throughout the seasons.

6 Discussion and conclusion

Infrasound data from ARCI have been processed by evaluating the Fisher ratio over the period of March 13, 2008 up to May 14, 2009. With a detection threshold at a SNR of 1, 1.8 million events are detected between 0.1 and 1.0 Hz and 16,475 events between 1.0 and 7.0 Hz. Detections in the low-frequency band are mostly related to the interaction of oceanic waves which leads to microbaroms. In the high-frequency band, mainly man-made events are detected which are related to mining and military activity. Similar findings have been reported by Le Pichon et al. (2008).

The characteristics of the medium, i.e., wind and temperature structure up to stratospheric altitudes, and the source have been derived from ECMWF models. A clear relation has been shown between upper atmospheric winds and the directionality of the detections for the low-frequency band. These seasonal changes are also partly visible in the high-frequency band. In winter, the sources to the west are detected while preference is given to sources in the east during summer. The state of the boundary layer, or turbulence and low-level winds, partly determines the signal coherency. In summer, there is a daily variation caused by the influence of solar radiation. A more stable boundary layer during nighttime leads to less coherency loss.

In addition, microbarom activity has been estimated by evaluating the ocean wave height and period. ARCI is sensitive to microbaroms from the Atlantic Ocean in winter. Microbarom energy from the east is detected during summer. This anisotropic behavior was also identified during a period of only a couple of days, related to a SSW. A sudden change was noted from the detection of microbarom energy from the Atlantic Ocean to those from the Pacific Ocean.

The importance of taking into account both the characteristics of the medium and the source is illustrated by comparing Figs. 5 and 8. The detections move from west (270°) to northwest (330°) during March and April 2008. It follows from Fig. 8 that the sources, microbaroms in the Atlantic Ocean, are occurring with a more or less stable backazimuth between 270° and 300°. The stratospheric wind, on other hand, is varying from southwest to north during this period. Therefore, this change in the resolved backazimuths should be attributed to the wind which enables the detection of an unknown source to the south of ARCI.

Another change is visible, in Fig. 8, between October 2008 and April 2009. The resolved backazimuths tend to move somewhat from the northwest to the west. The cause should be related to the source, as the wind shows no evidence for such translation. Whether this change relates to the southward movement of sea ice during winter remains to be investigated. It is hypothesized that the sea ice blocks the northward propagation of oceanic waves. Consequently, the generation of microbaroms is limited up to a certain longitude. This is also indicated by the microseism detections. The source seems limited in its northward propagation during winter (see Fig. 10).

The seasonal variations in microbarom detections also follow from the comparison with the microseismic detections. The highly dynamic and anisotropic nature of the atmosphere can prohibit the detection of energy from certain directions. The ocean wave activity, i.e., generation of microseism, is almost continuously present from the Atlantic and Pacific Ocean. The microbaroms appear from 270° during winter, while the microseism have a dominant backazimuth of 240°. The latter direction coincides with the location found by Essen et al. (2003) which was just off coast of Norway. The microbaroms are probably generated in the deep ocean as the direction points to a location similar to the one found by Evers and Haak (2001) and Kedar et al. (2008), which was in a region to the south of Greenland and Iceland. Further research will be carried out to determine the origin of the microseism and correlate those to microbaroms. Better statistics will be obtained by evaluating more than 1 year of data, by excluding, for example, special weather conditions.

In conclusion, the general behavior of an infrasound array, like ARCI, can be understood by evaluating the detectability in relation to atmospheric processes and source activity. Upper atmospheric winds and the state of the boundary layer play an important role in the detectability of infrasound. Understanding such dependencies is important for the identification of small-sized nuclear test which are expected to occur in the low-frequency or microbarom band.

Acknowledgements The work performed in this study was supported by a Transnational Access (TA) grant. This TA grant was provided by NERIES, an EC project with contract number RII3-CT-2006-026130. Figures in this article were made with the Generic Mapping Tools (Wessel and Smith 1991).

References

Balachandran NM, Donn WL, Rind D (1977) Concorde sonic booms as an atmospheric probe. Science 197:47–49

Dahlman O, Mykkeltveit S, Haak H (2009) Nuclear test ban. Springer, Dordrecht

Drob DP, Picone JM, Garcés MA (2003) The global morphology of infrasound propagation. J Geophys Res 108:4680

Essen HH, Krüger F, Dahm T, Grevemeyer I (2003) On the generation of secondary microseisms observed in northern and central Europe. J Geophys Res 108:2506

Evers LG, Haak HW (2001) Listening to sounds from an exploding meteor and oceanic waves. Geophys Res Lett 28:41–44

Evers LG, Haak HW (2005) The detectability of infrasound in the Netherlands from the Italian volcano Mt. Etna. J Atmos Sol-Terr Phys 67:259–268

Evers LG, Siegmund P (2009) Infrasonic signature of the 2009 major sudden stratospheric warming. Geophys Res Lett 23:L23,808

Garcés MA, Willis M, Hetzer C, Le Pichon A, Drob D (2004) On using ocean swells for continuous infrasonic measurements of winds and temperature in the lower, middle, and upper atmosphere. Geophys Res Lett 31:L19,304

Gossard EE, Hooke WH (1975) Waves in the atmosphere. Elsevier Scientific, Amsterdam

Hedlin MAH, Alcoverro B, D'Spain G (2003) Evaluation of rosette infrasonic noise-reducing spatial filters. J Acoust Soc Am 114:1807–1820

Holton JR (1979) An introduction to dynamic meteorology. Academic, London

Kedar SM, Longuet-Higgins MS, Webb F, Graham N, Clayton R, Jones C (2008) The origin of deep ocean microseisms in the North Atlantic Ocean. Proc R Soc Lond A 464:777–793

Le Pichon A, Ceranna L, Garés M, Drob D, Millet C (2006) On using infrasound from interacting ocean swells for global continuous measurements of winds and temperature in the stratosphere. J Geophys Res 111: D11,106

Le Pichon A, Vergoz J, Herry P, Ceranna (2008) Analyzing the detection capability of infrasound arrays in central Europe. J Geophys Res 113:D12,115

Le Pichon A, Vergoz J, Blanc E, Guilbert J, Ceranna L, Evers LG, Brachet N (2009) Assessing the performance of the international monitoring system infrasound network: geographical coverage and temporal variabilities. J Geophys Res 114:D8112

Liszka L (1978) Long-distance focusing of concorde sonic boom. J Acoust Soc Am 64:631–635

Melton BS, Bailey LF (1957) Multiple signal correlators. Geophysics XXII:565–588

Posey JW, Pierce AD (1971) Estimation of nuclear explosion energies from microbarograph records. Nature 232:253

Posmentier ES (1967) A theory of microbaroms. Geophys J R Astron Soc 13:487–501

Roth M, Fyen J, Larsen PW (2008) Setup of an experimental infrasound deployment within the ARCES array. Scientific Report 2-2008, NORSAR

Smart E, Flinn EA (1971) Fast frequency–wavenumber analysis and Fisher signal detection in real-time infrasonic array data processing. Geophys J R Astron Soc 26:279–284

Sutherland LC, Bass HE (2004) Atmospheric absorption in the atmosphere up to 160 km. J Acoust Soc Am 115:1012–1032

Symons GJ (ed) (1888) The eruption of Krakatoa and subsequent phenomena. Trübner & Co., London

Wessel P, Smith WHF (1991) Free software helps map and display data. EOS Trans AGU 72:441

Whipple FJW (1930) The great Siberian meteor and the waves, seismic and aerial, which it produced. Q J R Meteorol Soc 56:287–304

Whipple FJW (1939) The upper atmosphere, density and temperature, direct measurements and sound evidence. Q J R Meteorol Soc 65:319–323

AUTHOR QUERY

AUTHOR PLEASE ANSWER QUERY

Q1. Figures 5–8 were rasterized. Please check if captured appropriately.